Science Bulletin 64 (2019) 331–336

Contents lists available at ScienceDirect

Science Bulletin

journal homepage: www.elsevier.com/locate/scib

Article

Surface multiferroics in silicon enabled by hole-carrier doping

Xiaoyu Xuan, Wanlin Guo *, Zhuhua Zhang *

State Key Laboratory of Mechanics and Control of Mechanical Structures, Key Laboratory for Intelligent Nano Materials and Devices of Ministry of Education and Institute of Nanoscience, Nanjing University of Aeronautics and Astronautics, Nanjing 210016, China

ARTICLE INFO

Article history:
Received 11 December 2018
Received in revised form 24 January 2019
Accepted 12 February 2019
Available online 14 February 2019

Keywords:
Si(0 0 1)
Ferromagnetism
Electric dipole
Carrier doping
Ab initio calculations

ABSTRACT

We predict a coexistence of magnetic and electric orders on clean Si(0 0 1) surfaces by first-principles calculations. Upon hole-carrier doping, the Si surfaces can be ferromagnetic, with polarized spins concentrated in an atom-thick space near the surface, due to an exchange splitting of localized s-like surface states on surface Si dimers. The surface magnetization can be controlled by reorienting the electric polarization of Si dimers, manifested as a transition from the magnetic antiferroelectric ground state to ferroelectric $p(2 \times 1)$ reconstruction that can be driven by an in-plane external electric field. The coupling between magnetic and electric orders can be further enhanced by strain silicon technology, rendering the Si surfaces as the first metal-free material displaying a multiferroic behavior.

1. Introduction

Silicon reigns over current semiconductor technology due to its desirable band gap, earth abundance, and high carrier mobility. The roadmap of semiconductor technology has been strictly following the development of Si-based logic devices [1,2]. Yet, as the dimension of device scales down to several nanometers, how the Moore's Law continues has been of major and ongoing interests. One of promising solutions is to integrate logic operation and information storage within an individual device. Such integration necessitates the introduction of spin-polarization in nonmagnetic silicon and will be particularly efficient if the spins could be controlled by electric means. A number of experiments have demonstrated electric injection of polarized spins into silicon from a ferromagnetic metal spaced by a tunnel barrier [3–5], but the low spin-polarization and short spin lifetime limit the applications. Alternatively, considerable research efforts have been devoted to direct creation of intrinsic magnetism in silicon. One way is to introduce magnetic metals into silicon [6,7], which can induce high spin-polarization but tend to form clusters or secondary phases that impair the formation of magnetic order evenly distributed in the materials. Another way is to magnetize silicon itself by creating spin-polarized dangling bond states on H-terminated Si(111) surfaces [8] and clean Si(111) surfaces via metastable reconstruction [9] or chemisorption of graphene nanoribbons [10]. However, the as-induced magnetism not only is difficult for control but also requires sophisticated methods for realizing a specific network of dangling bonds that remain elusive. Fundamental questions thus arise, is it possible to create magnetism in a natural Si structure? If so, how can it be electrically controlled?

As a prototype of semiconductor surfaces, Si(001) surface has attracted great interest [11–15]. This surface is featured by its reconstruction via dimerization of the topmost atoms, which diminishes the dangling bonds to enhance the surface's stability [16–18]. Each Si dimer is buckled, consisting of a sp^2-like bonded "down" atom closer to the plane of its three neighbors underneath and a sp^3-like bonded "up" atom further away from the plane (Fig. 1a) and is electrically polarized due to charge transfer from the "down" to the "up" atom. The "up" atom contains an *s*-like surface state that is highly localized on the top of valence bands (Fig. 1b), in contrast to other dispersive surface and bulk states. Here, we employ such unique localized surface state, which can be triggered to be spin-polarized by doping hole carriers and consequently create substantial, uniform magnetism on the Si(001) surface, as demonstrated by first-principles calculations. Remarkably, the surface magnetization exhibits a nontrivial coupling with the electric polarization of Si dimers, thereby enabling a control of magnetism by an external electric field. These results extend the desired magnetoelectric (ME) effect into widely used Si nanostructures and will inspire the discovery of magnetoelectricity in other semiconductors based on charge carrier doping.

* Corresponding authors.
E-mail addresses: wlguo@nuaa.edu.cn (W. Guo), chuwazhang@nuaa.edu.cn (Z. Zhang).

https://doi.org/10.1016/j.scib.2019.02.006
2095-9273/

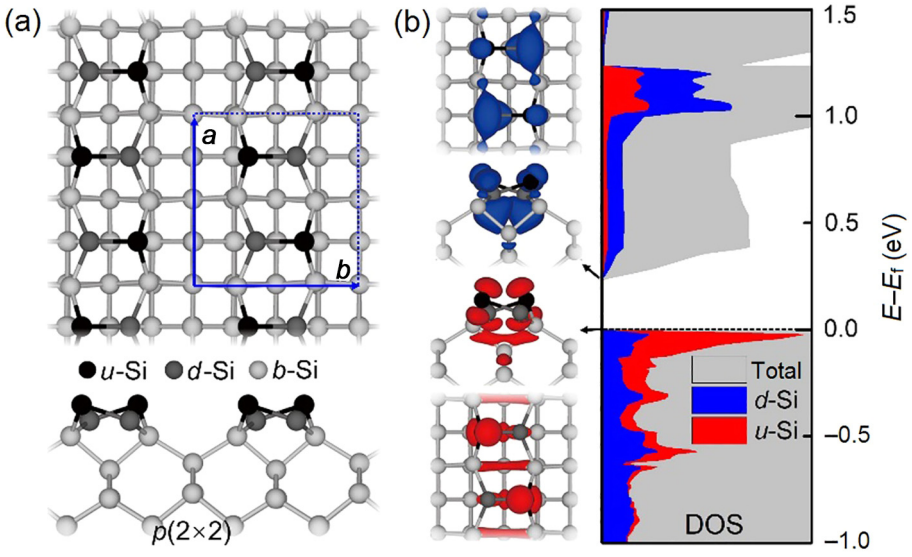

Fig. 1. (Color online) Structural and electronic features of a Si(001) reconstructed surface. (a) Top and side views of the surface. The dashed rectangle marks the surface's primitive cell. (b) Density of states of the surface, with contribution from the *d*- and *u*-Si atoms highlighted in blue (dark grey) and red (grey), respectively. The left insets are isosurface plots (0.02 e/Å^3) of charge densities corresponding to the valence band maximum (red or grey) and conduction band minimum (blue or dark grey), respectively.

2. Methods

Calculations were performed using ultrasoft pseudopotentials for the core region and spin-polarized density functional theory based on the generalized gradient approximation (GGA) of PBE functional [19], as implemented in the Vienna ab-initio simulation package (VASP) code [20,21]. We set a kinetic energy cutoff of 530 eV for the plane-wave expansion. The Si(001) surfaces were simulated using slab model, comprised of four Si double-layers and one layer of H atoms passivating the bottom Si atoms. A vacuum region of 15 Å was set to isolate neighboring periodic images and the Brillouin-zone was densely sampled. The atomic positions, except for the bottom Si atoms and the joint H atoms, were relaxed using conjugate-gradient method until the force on each atom was less than 0.01 eV/Å. The carrier doping was simulated by adjusting the charge-neutrality level with a jellium model. In experiments, the carrier doping could be realized using a field effect method that tunes the doping level continuously and the limit of doping level can be greatly enhanced by recently developed liquid gating technology [22]. We chose the $p(2 \times 2)$ structure as a reference phase to evaluate spontaneous electric polarization of the $p(2 \times 1)$ structure with modern Berry phase method. The external electric field E was modeled with a sawtooth potential applied across the dimer rows (Fig. S1 online).

3. Results and discussion

The buckled dimers on the Si surface tend to form parallel rows for minimizing the surface stress, and they alternate in the buckling direction along the rows. Across the dimer rows, the surface reconstructs in two ways: the buckling occurs in phase across the rows, denoted as $p(2 \times 2)$ (Fig. 1a), and the buckling phase shifts between adjacent rows, denoted as $c(4 \times 2)$ (Fig. S2 online). The $c(4 \times 2)$ structure is more stable by 2.6 meV/dimer than the $p(2 \times 2)$ one, but they share nearly the same electronic structure, thus holding similar magnetic responses to carrier doping. We primarily focus on the $p(2 \times 2)$ structure with lattice constants a = 7.85 Å and b = 7.69 Å and discuss the $c(4 \times 2)$ structure later. For ease of discussion, we use notation *u*- and *d*-Si to describe the "up" and "down" Si atoms in a dimer, respectively. The buckling can also occur in phase both along and across the dimer rows, forming a structure referred to as $p(2 \times 1)$ that is distinctly less stable than the $p(2 \times 2)$ one but possesses an intrinsic in-plane electric polarization, as discussed later.

On the Si(001) surface, the *d*-Si adopts a sp^2-like back bond while the *u*-Si possesses a more sp^3-like back bond, due to electron transfer from the *d*-Si to the *u*-Si. As a result, the surface state from the *d*-Si has a *p*-like distribution and is located at the conduction band minimum (CBM), whereas that from the *u*-Si is *s*-like and appears at the valence band maximum (VBM), as illustrated in Fig. 1b and insets. A band gap of 0.24 eV separates the *p*- and *s*-like surface bands and the surface is inherently nonmagnetic. However, the *s*-like surface state is highly localized with a sharp quasi-1D van Hove singularity near the VBM, suggesting a possibility of magnetic instability upon shifting the Fermi level downward by applying, for example, a gate voltage.

The Si(001) surface does become magnetic when the Fermi level cuts the *s*-like surface state under the hole-carrier doping. As shown by the bottom inset in Fig. 2a, the ground-state spin density of the surface at a doping level q = +6.62 × 10^{13} cm^{-2} is dominated by the *u*-Si atoms and has a little contribution from the *d*-Si atoms. The spin density decays rapidly toward the bulk lattice, rendering the system as a two-dimensional (2D) spin electron layer overlaid on a three-dimensional (3D) semiconducting host. The total magnetic moment reaches 0.29 μ_B/nm^2 (μ_B is the Bohr magneton), to which each *u*-Si atom contributes 0.043 μ_B. Test calculations using HSE06 functional give an even higher magnetic moment of 0.66 μ_B/nm^2 at the same doping level. In contrast, doping electrons to the surface results in a nonmagnetic ground state regardless of the doping level, as expected from the dispersive CBM derived from *d*-Si atoms. The hole-induced magnetism is found absent on diamond and Ge(001) surfaces, suggesting that the exchange interaction of surface states required for spin-splitting is uniquely strong for silicon. The magnetism is also found applicable to chemical doping sources, such as halogen and boron doping.

The magnetic moment per unit surface area, M, increases almost linearly with the doping level, from 0.05 μ_B/nm^2 at +3.31 × 10^{13} cm^{-2} to 0.76 μ_B/nm^2 at + 13.2 × 10^{13} cm^{-2}, as shown by the black line in Fig. 2a. The magnetic moment reaches a maximum of 1.4 μ_B/nm^2 at q = +23.2 × 10^{13} cm^{-2}, beyond which the Si surface undergoes significant structural distortion that reduces the

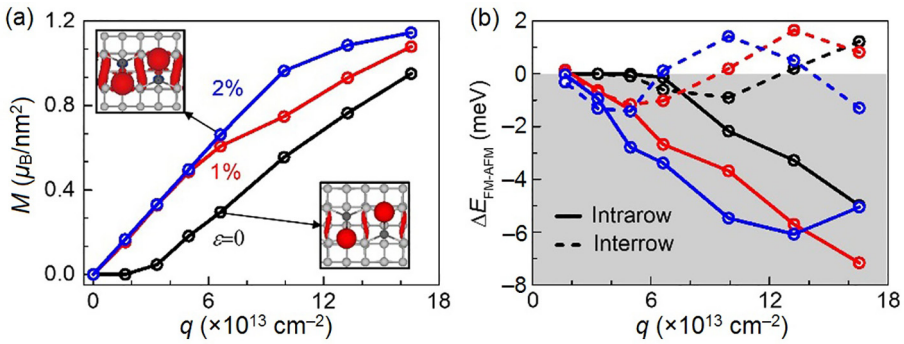

Fig. 2. (Color online) Magnetism of the Si(001) surface. (a) Magnetic moment as a function of carrier density q at different biaxial strains ε. The insets are isosurface plots (0.0027 e/Å^3) of spin density distributions at $q = +6.62 \times 10^{13}$ cm^{-2} with $\varepsilon = 0$ and 2%. (b) Exchange energy as a function of q at different ε. The solid and dashed lines strand for the spin coupling along and across the dimer rows, respectively.

magnetism abruptly thereafter (not shown). The distortion is manifested as the decline of u-Si to the same height of the d-Si and therefore eliminates the localized surface states necessary for the magnetism. At this point, the magnetic moment induced by each carrier reaches 0.61 μ_B, along with spin-polarization energy up to 23.4 meV per unit cell. On the other side, there is a critical doping level of $+3.31 \times 10^{13}$ cm^{-2}, below which the Si(001) surface stays nonmagnetic. This is because the s-like surface state partly overlaps with the dispersive bulk states near the VBM so that the Stoner criteria [23] required for the magnetic instability cannot be satisfied at small q.

Motivated by strain Si technology, we biaxially stretch the surface so that the s-like surface state is lifted with respect to the bulk bands due to their different deformation potentials [15]. Then, the hole carriers entirely populate the localized surface state to get fully spin-polarized. Indeed, the Si surface under a tensile strain $\varepsilon = 1\%$ is instantly magnetic as soon as hole carriers are introduced (Fig. 2a). In particular, we observe an evident proportionality between M and q, expressed as $M = 0.06q$ when $q \leq 6.62 \times 10^{13}$ cm^{-2}. At higher q, M falls off from the proportionality once the bulk-derived states are involved in carrier populating. An applied 2% tensile strain can sustain the proportionality to a higher level of $q = +9.9 \times 10^{13}$ cm^{-2} (Fig. 2a). Note that M increases with the strain in the nonlinear region.

We then examine the spin coupling strength by considering three magnetic orderings: (1) ferromagnetic ordering (FM), antiferromagnetic ordering with the spin direction alternated along the dimer row but occurred in phase across the rows (AFM_1), and antiferromagnetic ordering with the spin direction aligned along the dimer row but flipped across the rows (AFM_2) (Fig. S3 online). With no strain, the FM structure is energetically preferred below $q = +1.32 \times 10^{14}$ cm^{-2}, above which the AFM_2 structure becomes the ground state (Fig. 2b). The energy difference ΔE_{FM-AFM_1} decreases with increasing q and reaches −5.0 meV at $q = +16.5 \times 10^{14}$ cm^{-2} whereas ΔE_{FM-AFM_1} decreases first and then increases when $q > +13.2 \times 10^{14}$ cm^{-2}, yet its absolute value is less than 1.3 meV (Fig. 2b). Applied tensile strain increases $|\Delta E_{FM-AFM_1}|$, which reaches −7.16 meV at $\varepsilon = 1\%$ and $q = +16.5 \times 10^{14}$ cm^{-2}. In contrast, $|\Delta E_{FM-AFM_2}|$ is no larger than 3.3 meV within the studied range of strain. These results suggest that the FM coupling along dimer rows is much stronger than that across the rows. Thus, the dimer rows behave more like an array of FM chains settled on a Si substrate.

Employing Monte Carlo simulation at a mean field level (Fig. S4 online), we estimate the Curie temperature T_C for the magnetic surface, which is 15 K at $q = +8.27 \times 10^{13}$ cm^{-2} and rises to 94 K at $\varepsilon = 1.5\%$ and $q = +1.65 \times 10^{14}$ cm^{-2}. The latter is comparable to T_C in other metal-free magnetic systems, e.g., pristine Si(111)-$\sqrt{3}$ surface [9] and hole-doped 2D GaSe [24].

Aside from the magnetism, the Si(001) surface can deliver intriguing electric orders due to the buckled dimers. As discussed above, each dimer carries an electric dipole pointing from the u-Si to the d-Si. Ferroelectric behavior will emerge on the Si surface as long as the electric polarization of the dimer is switchable. Since the electrically polarized dimers are free to flip its buckling direction, the switch of polarization can be driven by an in-plane electric field, E_{ext}, applied transversely to dimer rows. The field-induced alignment of dimer buckling will transform the Si surface from the antiferroelectric $p(2 \times 2)$ structure to a ferroelectric $p(2 \times 1)$ one with a collective in-plane polarization.

Indeed, the relative energy, $\Delta E_{22\text{-}21}$, between the $p(2 \times 2)$ and $p(2 \times 1)$ structures depends on E_{ext} and q. Without an applied electric field, the charge-neutral $p(2 \times 2)$ structure is more stable than the $p(2 \times 1)$ one by 75 meV/dimer (Fig. 3a). An applied electric field can help stabilize the $p(2 \times 1)$ structure, which stays at the ground state when $E_{ext} = 0.55$ V/Å. The ferroelectric switch can be further facilitated by doping hole carriers and applying tensile strain. For $E_{ext} = 0.55$ V/Å, $\Delta E_{22\text{-}21}$ increases to 5.8 meV/dimer at $q = +4.96 \times 10^{13}$ cm^{-2} and further to 9.6 meV/dimer at an additional $\varepsilon = 2\%$. Since the relative stability between the two structures is dominated by the electrostatic interaction among the dimers, we analytically express $\Delta E_{22\text{-}21}$ by treating the surface as a 2D lattice of dipoles and summarizing their electrostatic energy based on tight-binding approximation (Fig. S5 online). By fitting to DFT results, we obtain

$$\Delta E_{22\text{-}21} = -0.15 + 0.28E_{ext} + 0.011q - 0.01E_{ext}q. \quad (1)$$

Eq. (1) is then used to plot a phase diagram for the Si(001) surface. The contours for $\Delta E_{22\text{-}21}$ in the entire E_{ext}–q parameter space shows that the field-induced transition from the nonpolar $p(2 \times 2)$ to the polar $p(2 \times 1)$ structure can be well aided by the hole carrier doping and that the coercive field decreases with increasing q (Fig. 3b), down to 0.24 V/Å at $q = +8.27 \times 10^{13}$ cm^{-2}. In addition to the relative stability, the kinetic barrier for the transition can be evidently reduced by the doping and electric field. The barrier for the $p(2 \times 2)$-to-$p(2 \times 1)$ transition is 0.24 eV in the pristine case, decreases to 0.15 eV at $E_{ext} = 0.55$ V/Å, and further down to 0.09 eV at $E_{ext} = 0.55$ V/Å and $q = +4.96 \times 10^{13}$ cm^{-2} (Fig. 3a).

Using the Berry phase method, the electric polarization of charge-neutral $p(2 \times 1)$ structure is calculated to be 3.66×10^{-10} C/m at charge neutrality, higher than the reported values for other 2D materials with ferroelectric order, e.g., SnSe [25], Te [26], P_2O_3 [27] and Bi [28]. Since the Berry phase method cannot be applied to a system with metallic bands, we calculate the dipole

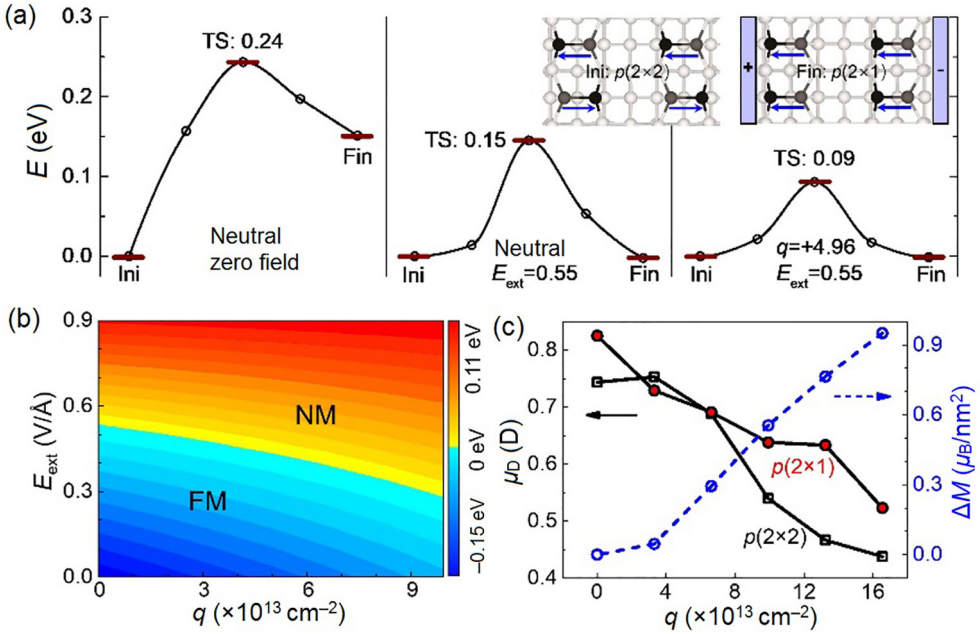

Fig. 3. (Color online) Ferroelectric switch of the Si(001) surface. (a) Calculated energy along the minimum energy paths between the $p(2 \times 2)$ and $p(2 \times 1)$ reconstructions at pristine state (left), with E_{ext} = 0.55 V/Å (middle), with $q = +4.96 \times 10^{13}$ cm^{-2} and E_{ext} = 0.55 V/Å (right). Insets illustrate the electric dipoles on Si dimers and their ferroelectric switch by external electric fields. (b) Phase diagram of the surface reconstruction based on the energy difference between the $p(2 \times 2)$ and $p(2 \times 1)$ structures as a function of q and E_{ext}. Possible coexistence of magnetic and electric orders is also given. (c) Dipole moment per dimer on the $p(2 \times 2)$ and $p(2 \times 1)$ structures as well as the magnetic moment difference between the $p(2 \times 2)$ and $p(2 \times 1)$ structures as functions of hole carrier density.

moment of each dimer, μ_D, for the hole-doped Si surfaces, as shown in Fig. 3c. The results show that μ_D decreases with increasing q and still can be 0.64 D even at $q = +9.93 \times 10^{13}$ cm^{-2}. The existence of electric polarization on the hole-doped surface is unusual and attributed to an inefficient screening of the highly localized surface bands. Indeed, the dimers on the $p(2 \times 1)$ structure are persistently buckled at various doping levels, along with a charge asymmetry between two atoms. Thus, the electric dipoles of dimers remain electrically controllable even when the system is doped by hole carriers, as shown in Fig. 3a. Note that electric dipoles have also been reported in boron-deficient MgB_6 that possesses a finite density of states at the Fermi level [29].

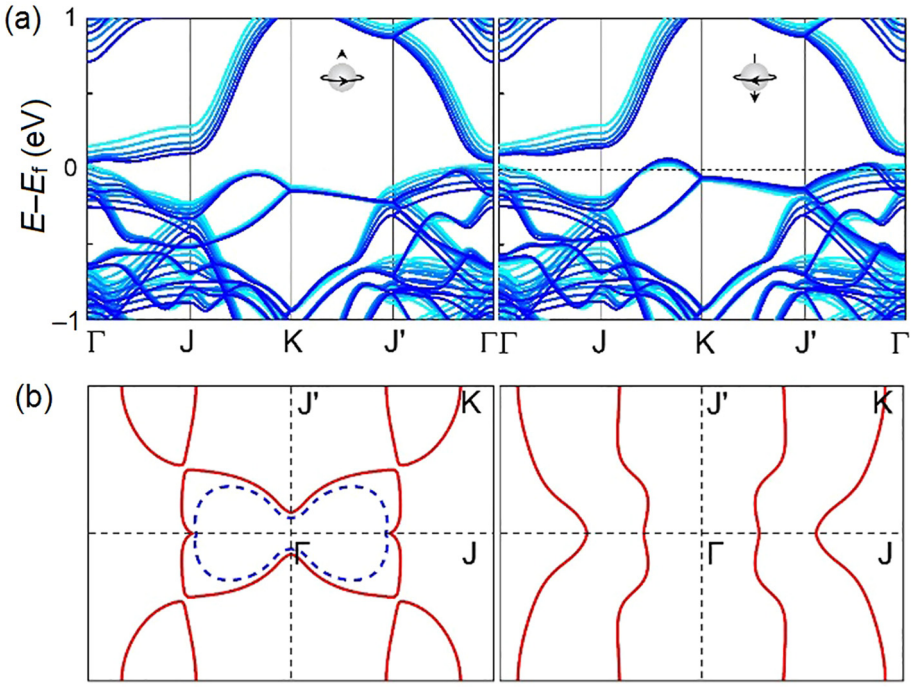

Fig. 4. (Color online) Electronic properties of the $p(2 \times 2)$ reconstructed Si(001) at $q = 6.62 \times 10^{13}$ cm^{-2}. (a) Spin-polarized band structure under different ε from 0% (cyan or light grey) to 2% (blue or dark grey); Left is for the spin-up and right for the spin-down channel. (b) Fermi surfaces at $\varepsilon = 0$ (left) and 2% (right). Dotted and solid lines stand for the spin-up and spin-down channels, respectively.

The coexistence of electric polarization and ferromagnetism on the hole-doped Si(001) surface raises an intriguing question as to whether the two orders can couple with each other to induce a ME effect. We thus examine the change of magnetism induced by the ferroelectric switch. The ferroelectric $p(2 \times 1)$ structure turn out to be nonmagnetic in the studied range of carrier doping, attributed to its delocalized *s*-like surface state near the VBM. The variation of magnetic moment, ΔM, is 0.42 μ_B/nm^2 at $q = 8.27 \times 10^{13}$ cm^{-2}, with a coercive field of $E_{ext}^{cor} = 0.16$ V/Å. The ME coefficient estimated by $\alpha_S = \mu_0 \Delta M / E_{ext}^{cor}$ reaches 1.5×10^{-13} G cm^2/V, an order of magnitude higher than those of FM metal films [30] and comparable to those in graphene nanoribbons under a bias voltage [14]. This ME coefficient can be further enhanced by the applied elastic strain. For example, at $\varepsilon = 2\%$, E_{ext}^{cor} is reduced to 0.1 V/Å while ΔM rises to 0.83 μ_B/nm^2, resulting in a larger α_S of 4.75×10^{-13} G cm^2/V. The Si(001) surface thus appears to be a peculiar system displaying strong mechan-electro-magnetic coupling. In contrast to reported ME systems [30–39], the ME coupling of the Si(0 0 1) stems from a change in electronic localization induced by ferroelectric displacement. This mechanism ends up a nonlinear ME effect on the surface. We obtain similar results for the ferroelectric switch between the $c(4 \times 2)$ and $p(2 \times 1)$ structures, as the $c(4 \times 2)$ structure has essentially the same electric order to the $p(2 \times 2)$ structure.

The ME Si surface exhibits two compelling electronic features. First, as the surface bands are isolated from the bulk states by the tensile strain, a half-metallic nature appears on the hole-doped Si surface: the conductive bands are only from the spin-down channel (Fig. 4a). The spin transport will benefit from relatively dispersive conductive bands and a sizable band gap of 65 meV ($\varepsilon = 2\%$) in the spin-up channel. Second, the surface exhibits two hole pockets, one is in the K-J path and the other in the Γ-J' path. The first pocket carries holes only in the spin-down channel while the second does in both spin channels. At $\varepsilon = 2\%$, the two pockets are in the spin-down channel, along with an evolution of their shapes from a ring to a quasi-rectangle (Fig. 4b). The change in the topology of Fermi surface may cause a nesting instability at certain doping levels.

These electronic features indicate that transistor devices made of the ME Si surface allow the process of logic information with low energy consumption and excellent compatibility with traditional technologies. Selectively passivating Si dimers with H atoms can turn the system into a magnetoelectric-semiconducting "hetero-structure". The atomically smooth interface in such a heterostructure will facilitate spin injection into the semiconducting regions and lead to new devices, e.g., spin diodes. An additional advantage of the spin injection will lie at the control by ferroelectric switch. Further thinning the magnetic region to a single dimer row would allow for the fundamental study of ME behavior in 1D space.

4. Conclusion

In conclusion, our first-principles calculations have presented an unexpected coexistence of ferromagnetic and electric orders on hole-doped Si(001) surfaces. The ferromagnetism stems from strongly localized *s*-like surface states on the sp^3-bonded surface Si atoms near the valence band top while the electric order is attributed to switchable electric polarization of Si dimers. Notably, the ferromagnetism and electric polarization are strongly coupled to render the surface as the first Si material enabling an electric control of its surface magnetization. Moreover, the ME coupling can be further regulated by an applied elastic strain and selective chemical passivation to allow for new spintronic applications.

Conflict of interest

The authors declare that they have no conflict of interest.

Acknowledgments

This work was supported by the National Natural Science Foundation of China (11772153, 51535005, and 51472117), the Research Fund of State Key Laboratory of Mechanics and Control of Mechanical Structures (MCMS-0417G01, MCMS-I-0418 K01, and MCMS-I-0418Y01), the Fundamental Research Funds for the Central Universities (NE2018002, NC2018001), and Youth Thousand Talents Program.

Author contributions

Xiaoyu Xuan performed the DFT calculation. Zhuhua Zhang contributed to data analysis and writing. Wanlin Guo and Zhuhua Zhang supervised the project. All authors discussed the results and commented on the manuscript.

Appendix A. Supplementary data

Supplementary data to this article can be found online at https://doi.org/10.1016/j.scib.2019.02.006.

References

[1] Schulz M. The end of the road for silicon? Nature 1999;399:729–30.
[2] Cowburn RP, Welland E. Room temperature magnetic quantum cellular automata. Science 2000;287:1466–8.
[3] Jonker BT, Kioseoglou G, Hanbicki AT, et al. Electrical spin-injection into silicon from a ferromagnetic metal/tunnel barrier contact. Nat Phys 2007;3:542–6.
[4] van't Erve OMJ, Hanbicki AT, Holub M, et al. Electrical injection and detection of spin-polarized carriers in silicon in a lateral transport geometry. Appl Phys Lett 2007;91:212109.
[5] Dash SP, Sharma S, Patel RS, et al. Electrical creation of spin polarization in silicon at room temperature. Nature 2009;462:491–4.
[6] Zhang FM, Liu XC, Gao J, et al. Investigation on the magnetic and electrical properties of crystalline $Mn_{0.05}Si_{0.95}$ films. Appl Phys Lett 2004;85:786–8.
[7] Bolduc M, Awo-Affouda C, Stollenwerk A, et al. Above room temperature ferromagnetism in Mn-ion implanted Si. Phys Rev B 2005;71:033302.
[8] Okada S, Shiraishi K, Oshiyama A. Magnetic ordering of dangling bond networks on hydrogen-deposited Si(111) surfaces. Phys Rev Lett 2003;90:026803.
[9] Fu H, Liu Z, Lian C, et al. Magnetic dirac fermions and chern insulator supported on pristine silicon surface. Phys Rev B 2016;94:035427.
[10] Yi JB, Lim CC, Xing GZ, et al. Ferromagnetism in dilute magnetic semiconductors through defect engineering: Li-doped ZnO. Phys Rev Lett 2010;104:137201.
[11] Seino K, Schmidt WG, Bechstedt F. Energetics of Si(001) surfaces exposed to electric fields and charge injection. Phys Rev Lett 2004;93:036101.
[12] Lu GH, Liu F. Towards quantitative understanding of formation and stability of Ge hut islands on Si(001). Phys Rev Lett 2005;94:176103.
[13] Yu SY, Kim H, Koo JY. Extrinsic nature of point defects on the Si(001) surface: dissociated water molecules. Phys Rev Lett 2008;100:036107.
[14] Zhang ZH, Chen CF, Guo WL. Magnetoelectric effect in graphene nanoribbons on substrates via electric bias control of exchange splitting. Phys Rev Lett 2009;103:187204.
[15] Zhou M, Liu Z, Wang Z, et al. Strain-engineered surface transport in Si(001): complete isolation of the surface state via tensile strain. Phys Rev Lett 2013;111:246801.
[16] Schlier RE, Farnsworth HE. Structure and adsorption characteristics of clean surfaces of germanium and silicon. J Chem Phys 1959;30:917–26.
[17] Chadi DJ. Atomic and electronic structures of reconstructed Si(100) surfaces. Phys Rev Lett 1979;43:43–7.
[18] Krüger P, Pollmann J. Dimer reconstruction of diamond, Si, and Ge (001) surfaces. Phys Rev Lett 1995;74:1155–8.
[19] Perdew JP, Burke K, Ernzerhof M. Generalized gradient approximation made simple. Phys Rev Lett 1996;77:3865.
[20] Kresse G, Hafner J. Ab initiomolecular-dynamics simulation of the liquid-metal–amorphous-semiconductor transition in germanium. Phys Rev B 1994;49:14251–69.
[21] Furthmuller GKJ. Efficient iterative schemes for ab initio total-energy calculations using a plane-wave basis set. Phys Rev B 1996;54:11169–86.

[22] Yuan H, Shimotani H, Tsukazaki A, et al. High-density carrier accumulation in ZnO field-effect transistors gated by electric double layers of ionic liquids. Adv Funct Mater 2009;19:1046–53.
[23] Stoner EC. Collective electron ferromagnetism. Proc R Soc Lond Ser A 1938;165:922.
[24] Cao T, Li Z, Louie SG. Tunable magnetism and half-metallicity in hole-doped monolayer GaSe. Phys Rev Lett 2015;114:236602.
[25] Fei R, Kang W, Yang L. Ferroelectricity and phase transitions in monolayer group-IV monochalcogenides. Phys Rev Lett 2016;117:097601.
[26] Wang Y, Xiao CC, Chen MG, et al. Two-dimensional ferroelectricity and switchable spin-textures in ultra-thin elemental te multilayers. Mater Horiz 2018;5:521–8.
[27] Luo W, Xiang H. Two-dimensional phosphorus oxides as energy and information materials. Angew Chem Int Ed Eng 2016;55:8575–80.
[28] Xiao CC, Wang F, Yang SYA, et al. Elemental ferroelectricity and antiferroelectricity in group-V monolayer. Adv Funct Mater 2018;28:1707383.
[29] Popov I, Baadji N, Sanvito S. Magnetism and antiferroelectricity in MgB_6. Phys Rev Lett 2012;108:107205.
[30] Seixas L, Rodin AS, Carvalho A, et al. Multiferroic two-dimensional materials. Phys Rev Lett 2016;116:206803.
[31] Duan CG, Jaswal SS, Tsymbal EY. Predicted magnetoelectric effect in Fe/$BaTiO_3$ multilayers: ferroelectric control of magnetism. Phys Rev Lett 2006;97:047201.
[32] Duan CG, Velev JP, Sabirianov RF, et al. Surface magnetoelectric effect in ferromagnetic metal films. Phys Rev Lett 2008;101:137201.
[33] Lee JH, Fang L, Vlahos E, et al. A strong ferroelectric ferromagnet created by means of spin-lattice coupling. Nature 2010;466:954–8.
[34] Wu M, Burton JD, Tsymbal EY, et al. Multiferroic materials based on organic transition-metal molecular nanowires. J Am Chem Soc 2012;134:14423–9.
[35] Yang Q, Xiong W, Zhu L, et al. Chemically functionalized phosphorene: two-dimensional multiferroics with vertical polarization and mobile magnetism. J Am Chem Soc 2017;139:11506–12.
[36] Zhang JJ, Lin LF, Zhang Y, et al. Type-ii multiferroic $Hf_2VC_2F_2$ mxene monolayer with high transition temperature. J Am Chem Soc 2018;140:9768–73.
[37] Zhao YH, Lin LF, Zhou QH, et al. Surface vacancy-induced switchable electric polarization and enhanced ferromagnetism in monolayer metal trihalides. Nano Lett 2018;18:2943–9.
[38] Huang C, Du Y, Wu H, et al. Prediction of intrinsic ferromagnetic ferroelectricity in a transition-metal halide monolayer. Phys Rev Lett 2018;120:147601.
[39] Liu K, Lu J, Picozzi S, et al. Intrinsic origin of enhancement of ferroelectricity in SnTe ultrathin films. Phys Rev Lett 2018;121:027601.

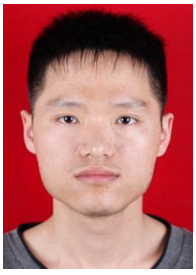

Xiaoyu Xuan received his Bachelor's degree from Nanjing University of Aeronautics and Astronautics in 2016. He joined the Institute of Nano Science at Nanjing University of Aeronautics and Astronautics in 2016. His current interest is electronic and magnetic properties of low-dimensional nanomaterials.

Zhuhua Zhang obtained his B.E. degree in 2004 and completed his Ph.D. research in 2010, both at Nanjing University of Aeronautics and Astronautics, China. He was a postdoctoral fellow at Rice University in 2012–2017. From May 2017, he started running a theoretical group at Nanjing University of Aeronautics and Astronautics. His current research interests include computational study of low-dimensional materials and liquid-solid interaction.

Wanlin Guo obtained his Ph.D. degree from Northwestern Polytechnical University in 1991, and in 2017 he was elected as an academician of the Chinese Academy of Science. He is a Chair Professor at Nanjing University of Aeronautics and Astronautics and the founding director of the Key Laboratory of Intelligent Nano Materials and Devices of Ministry of Education. His recent research interest includes physical mechanics of intelligent nanomaterials and devices, hydrovoltaics and brain-like artificial intelligence as well as mechanics of solids and structures.